Computers and Mathematics with Applications 68 (2014) 2167–2181

Contents lists available at ScienceDirect

Computers and Mathematics with Applications

journal homepage: www.elsevier.com/locate/camwa

A discrete Helmholtz decomposition with Morley finite element functions and the optimality of adaptive finite element schemes☆

Carsten Carstensen[a,*], Dietmar Gallistl[a], Jun Hu[b]

[a] Institut für Mathematik, Humboldt-Universität zu Berlin, Unter den Linden 6, D-10099 Berlin, Germany
[b] LMAM and School of Mathematical Sciences, Peking University, Beijing 100871, PR China

ARTICLE INFO

Article history:
Available online 12 August 2014

Keywords:
Discrete Helmholtz decomposition
Morley element
Kirchhoff–Love plate problem
Optimality

ABSTRACT

The discrete reliability of a finite element method is a key ingredient to prove optimal convergence of an adaptive mesh-refinement strategy and requires the interchange of a coarse triangulation and some arbitrary refinement of it. One approach for this is the careful design of an intermediate triangulation with one-level refinements and with the remaining difficulty to design some interpolation operator which maps a possibly nonconforming approximation into the finite element space based on the finer triangulation. This paper enfolds the second possibility of some novel discrete Helmholtz decomposition for the nonconforming Morley finite element method. This guarantees the optimality of a standard adaptive mesh-refining algorithm for the biharmonic equation. Numerical examples illustrate the crucial dependence of the bulk parameter and the surprisingly short pre-asymptotic range of the adaptive Morley finite element method.

1. Introduction

The biharmonic equation is the simplest and most classical fourth-order model in the computational mechanics of structures which has recently gained tremendous attention for the numerical simulation of implicit partial differential equations [1–3]. Since conforming finite element methods require C^1 conformity, the nonconforming approximation is highly popular in practice and its most prominent version is the Morley finite element method [4–6] with the space $M(\mathcal{T}_\ell)$ of piecewise quadratic shape functions on regular triangulations into triangles which are continuous at the nodes and have a vanishing integral of the jumps of the normal derivatives over interior edges, see Fig. 1.

The analysis of this paper is carried out for clamped boundary conditions where the space of admissible functions is the space $H^2_0(\Omega)$ of H^2 functions whose values and normal derivatives vanish along the boundary. The a priori error analysis makes use of a certain interpolation operator I_M and its additional properties and has recently been weakened in the regularity assumptions on the exact solutions in [7] where its quasi-optimality up to extra volume contributions is derived for weak solutions in $H^2_0(\Omega)$. The a posteriori error control is well developed in [8,9] with explicit residual-based error

☆ This work was supported by the Chinesisch-Deutsches Zentrum project GZ578. The first two authors were partially supported by the DFG Research Center MATEON through the project C22. The research of the third author was supported by the NSFC Project 10971005, partially supported by the NSFC Project 11271035 and by the NSFC Key Project 11031006.

* Corresponding author.
E-mail addresses: cc@math.hu-berlin.de (C. Carstensen), gallistl@math.hu-berlin.de (D. Gallistl), hujun@math.pku.edu.cn (J. Hu).

http://dx.doi.org/10.1016/j.camwa.2014.07.019
0898-1221/

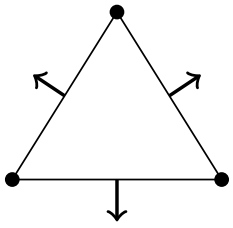

Fig. 1. Morley finite element.

estimators which may drive an automatic mesh-refining algorithm [10,11]. On each triangle T, the local error estimator contribution consists of a volume term plus tangential jumps of the discrete Hessian along the edges of T,

$$\eta_\ell^2(T) := \|h_T^2 f\|_{L^2(T)}^2 + \sum_{E\in\mathcal{E}(T)} h_E \|[D_{\mathrm{NC}}^2 u_\ell]_E \tau_E\|_{L^2(E)}^2.$$

The optimality proof follows the paradigm in [12] which has been extended and generalized in [13,14] to various kinds of second-order elliptic PDEs and in particular in [15–20] for nonconforming P_1 finite element schemes sometimes named after Crouzeix–Raviart. The key argument for optimality is the discrete reliability

$$|||u_\ell - u_{\ell+m}|||_{\mathrm{NC}}^2 \le C_{\mathrm{drel}} \eta_\ell^2(\mathcal{T}_\ell \setminus \mathcal{T}_{\ell+m}). \tag{1.1}$$

It states that the energy difference of two solutions u_ℓ and $u_{\ell+m}$ related to triangulations $\mathcal{T}_\ell$ and $\mathcal{T}_{\ell+m}$ from two different levels of the adaptive algorithm can be controlled by the error estimator contributions of the triangles in $\mathcal{T}_\ell \setminus \mathcal{T}_{\ell+m}$ with a constant C_{drel} that does not depend on m.

There is a proof for (1.1) by a transfer operator in [11]. The main idea therein is to modify the function u_ℓ only on the triangles $\mathcal{T}_\ell \setminus \mathcal{T}_{\ell+m}$. It employs the canonical interpolation of the quasi-interpolation by the conforming Hsieh–Clough–Tocher finite element in the region that consists of all refined triangles which have a positive distance from the unrefined region $\mathcal{T}_\ell \cap \mathcal{T}_{\ell+m}$ and some mixture in the layer between this region and $\mathcal{T}_\ell \setminus \mathcal{T}_{\ell+m}$. However, in the published version of [11, Lemma 5.9], it is unclear whether the intermediate interpolation operator in that layer is uniformly bounded with respect to m for some very special configurations. Although that small detail was fixed with a minor variation of the transfer operator in the version of [21], this paper generalizes the usage of discrete Helmholtz decompositions [15,17,22] from second-order problems to fourth-order problems: Any piecewise constant symmetric tensor field σ_ℓ allows a stable decomposition into a discrete Hessian of a Morley FEM function $\phi_\ell \in M(\mathcal{T}_\ell)$ and the symmetric part of a Curl of a piecewise affine H^1 vector field ψ_ℓ. This property allows for an immediate proof of the aforementioned discrete reliability (1.1) and so for an optimality proof of the associated adaptive finite element method. This provides a simple alternative to the analysis in [11] and may have many future applications. A similar discrete Helmholtz decomposition was employed in [23] in the context of mixed finite element schemes for fourth-order problems.

The remaining parts of this paper are as follows. Section 2 introduces the adaptive Morley FEM along with the necessary notation on regular triangulations and function spaces. Section 3 states and proves the discrete Helmholtz decomposition and its variants. Section 4 establishes the discrete reliability. Section 5 presents the optimality result based on the concept of nonlinear approximation classes. Section 6 outlines a simple Matlab implementation of the Morley FEM. Section 7 presents numerical tests for several nonconvex domains and different bulk parameters.

Throughout the paper standard notation on Lebesgue and Sobolev spaces is employed. The integral mean is denoted by $\fint$; H^{-1} and $H^{-2}(\Omega)$ denote the dual spaces of $H_0^1(\Omega)$ and $H_0^2(\Omega)$. The space of smooth tensor fields with compact support in Ω is denoted by $\mathcal{D}(\Omega;\mathbb{R}^{2\times 2})$. The dot denotes the product of two one-dimensional lists of the same length while the colon denotes the Euclidean product of matrices, e.g., $a\cdot b = a^\top b \in \mathbb{R}$ for $a, b \in \mathbb{R}^2$ and $A : B = \sum_{j,k=1}^2 A_{jk}B_{jk}$ for 2×2 matrices A, B. The notation $a \lesssim b$ abbreviates $a \le Cb$ for a positive generic constant C that may depend on the domain Ω but not on the mesh-size. The notation $a \approx b$ stands for $a \lesssim b \lesssim a$. The measure $|\cdot|$ is context-sensitive and refers to the number of elements of some finite set or the length of an edge or the area of some domain and not just the modulus of a real number or the Euclidean length of a vector.

2. Preliminaries

This section presents the adaptive Morley FEM and departs with necessary notation on regular triangulations.

2.1. Triangulations and function spaces

Let $\Omega \subseteq \mathbb{R}^2$ be a bounded polygonal Lipschitz domain with outer unit normal ν. Let $\mathcal{T}_\ell$ be a regular triangulation of Ω, with edges $\mathcal{E}_\ell$ and vertices $\mathcal{N}_\ell$. The interior (resp. boundary) edges are denoted by $\mathcal{E}_\ell(\Omega)$ (resp. $\mathcal{E}_\ell(\partial\Omega)$). Analogously let $\mathcal{N}_\ell(\Omega)$ denote the interior vertices and $\mathcal{N}_\ell(\partial\Omega)$ denote the vertices on the boundary. The set of edges of a triangle $T \in \mathcal{T}_\ell$ reads $\mathcal{E}(T)$, the set of vertices of T is denoted by $\mathcal{N}(T)$. For any $T \in \mathcal{T}_\ell$ let $h_T = |T|^{1/2}$ and define the piecewise constant

mesh-size function h_ℓ by $h_\ell|_T := h_T$. The length of an edge $E \in \mathcal{E}_\ell$ is denoted by h_E. For any interior edge $E \in \mathcal{E}_\ell(\Omega)$, there exist two adjacent triangles T_+ and T_- such that $E = \partial T_+ \cap \partial T_-$ (see Fig. 2). Let $\nu_E = (\nu_E(1); \nu_E(2))$ denote the fixed normal vector of E that points from T_+ to T_-. For $E \in \mathcal{E}_\ell(\partial\Omega)$, let ν_E denote the outward unit normal vector of Ω. The tangential vector of an edge E is denoted by $\tau_E := (-\nu_E(2); \nu_E(1))$. Given any (possibly vector-valued) function v, define the jump and the average of v of across E by

$$[v]_E := v|_{T_+} - v|_{T_-} \quad \text{and} \quad \langle v\rangle_E := (v|_{T_+} + v|_{T_-})/2 \quad \text{along } E.$$

For a boundary edge $E \in \mathcal{E}_\ell(\partial\Omega) \cap \mathcal{E}(T_+)$, define $[v]_E := v|_E$ and $\langle v\rangle_E := v|_E$.

For any $T \in \mathcal{T}_\ell$, the space of polynomial functions of degree k is denoted by $P_k(T)$. The space of piecewise polynomials reads

$$P_k(\mathcal{T}) = \{v \in L^2(\Omega) \mid \forall T \in \mathcal{T}, v|_T \in P_k(T)\}.$$

Let $\mathbb{S} \subseteq \mathbb{R}^{2\times 2}$ denote the space of symmetric 2×2 matrices. Square-integrable functions with values in $\mathbb{R}^2$, $\mathbb{R}^{2\times 2}$ and $\mathbb{S}$ are denoted by $L^2(\Omega;\mathbb{R}^2)$, $L^2(\Omega;\mathbb{R}^{2\times 2})$ and $L^2(\Omega;\mathbb{S})$, respectively. The spaces of piecewise vector-valued or tensor-valued polynomials $P_k(\mathcal{T}_\ell;\mathbb{R}^2)$, $P_k(\mathcal{T}_\ell;\mathbb{R}^{2\times 2})$ and $P_k(\mathcal{T}_\ell;\mathbb{S})$ are defined analogously. Real-valued (resp. vector-valued) L^2 functions with vanishing integral mean over Ω are denoted by $L^2_0(\Omega)$ (resp. $L^2_0(\Omega;\mathbb{R}^2)$). The space of vector fields whose components are $H^1(\Omega)$ functions is denoted by $H^1(\Omega;\mathbb{R}^2)$. For $v \in H^1(\Omega;\mathbb{R}^2)$, the Curl reads

$$\operatorname{Curl} v := \begin{pmatrix} -\partial v_1/\partial x_2 & \partial v_1/\partial x_1 \\ -\partial v_2/\partial x_2 & \partial v_2/\partial x_1 \end{pmatrix}.$$

The symmetric and the deviatoric part of a 2×2 matrix are defined as $\operatorname{sym} A := (A + A^\top)/2$ and $\operatorname{dev} A := A - 1/2 \operatorname{tr}(A)\ 1_{2\times 2}$. The piecewise action of the differential operators ∇ and D^2 is denoted by ∇_{NC} and D^2_{NC}. The L^2 projection onto piecewise constants with respect to $\mathcal{T}_\ell$ is denoted by $\Pi_{0,\mathcal{T}_\ell} \equiv \Pi_{0,\ell}$.

2.2. Morley finite element discretization of the biharmonic equation

Given $f \in L^2(\Omega)$, the biharmonic problem seeks $u \in H^2(\Omega)$ with

$$\Delta^2 u = f \quad \text{in } \Omega \quad \text{and} \quad u = \frac{\partial u}{\partial \nu} = 0 \quad \text{on } \partial\Omega.$$

Its weak form utilizes the Hilbert space $V := H^2_0(\Omega)$, namely the closure of $\mathcal{D}(\Omega)$ with respect to the H^2 norm, and the bilinear form

$$a(v, w) := \int_\Omega D^2 v : D^2 w \, dx \quad \text{for all } v, w \in V$$

with induced norm $|||\cdot||| := a(\cdot,\cdot)^{1/2}$. The weak formulation seeks $u \in V$ such that

$$a(u, v) = \int_\Omega f v \, dx \quad \text{for all } v \in V \equiv H^2_0(\Omega). \tag{2.1}$$

The Morley finite element space reads

$$M(\mathcal{T}_\ell) := \Big\{ v \in P_2(\mathcal{T}_\ell) \mid v \text{ is continuous at the interior vertices and vanishes at the vertices of } \partial\Omega; \\ \nabla_{\mathrm{NC}} v \text{ is continuous at the interior edges' midpoints and vanishes at the midpoints of the edges of } \partial\Omega \Big\}.$$

The discrete version of the energy scalar product reads

$$a_{\mathrm{NC}}(v, w) := \int_\Omega D^2_{\mathrm{NC}} v : D^2_{\mathrm{NC}} w \, dx \quad \text{for all } v, w \in V + M(\mathcal{T}_\ell)$$

with induced discrete energy norm $|||\cdot|||_{\mathrm{NC}} := a_{\mathrm{NC}}(\cdot,\cdot)^{1/2}$. The Morley finite element discretization of (2.1) seeks $u_\ell \in M(\mathcal{T}_\ell)$ such that

$$a_{\mathrm{NC}}(u_\ell, v_\ell) = \int_\Omega f v_\ell \, dx \quad \text{for all } v_\ell \in M(\mathcal{T}_\ell). \tag{2.2}$$

2.3. Explicit residual-based error estimator

For any $T \in \mathcal{T}_\ell$, the explicit residual-based error estimator $\eta_\ell := \eta_\ell(\mathcal{T}_\ell)$ consists of the contributions

$$\eta_\ell^2(T) := \|h_T^2 f\|^2_{L^2(T)} + \sum_{E\in\mathcal{E}(T)} h_E \|[D^2_{\mathrm{NC}} u_\ell]_E \tau_E\|^2_{L^2(E)} \quad \text{for any } T \in \mathcal{T}_\ell,$$

$$\eta_\ell^2(\mathcal{K}) := \sum_{T\in\mathcal{K}} \eta_\ell^2(T) \quad \text{for any subset } \mathcal{K} \subset \mathcal{T}_\ell.$$

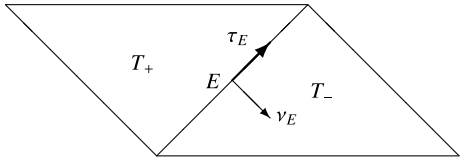

Fig. 2. Adjacent triangles T_- and T_+ that share the edge $E = \partial T_- \cap \partial T_+$.

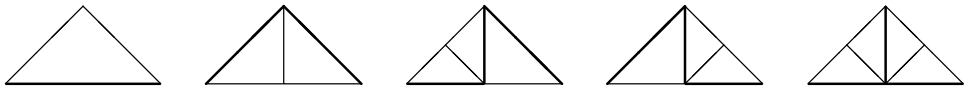

Fig. 3. Possible refinements of a triangle T in one level within the NVB. The thick lines indicate the refinement edges of the sub-triangles as in [24,25].

The global error estimator η_ℓ is known [8,9] to be reliable and efficient in the sense that there exist constants $C_{\rm rel} \approx 1 \approx C_{\rm eff}$ such that

$$C_{\rm rel}^{-1} |\!|\!| u - u_\ell |\!|\!|_{\rm NC}^2 \le \eta_\ell^2 \le C_{\rm eff} |\!|\!| u - u_\ell |\!|\!|_{\rm NC}^2 + {\rm osc}^2(f, \mathcal{T}_\ell) \tag{2.3}$$

where the oscillations read

$$ {\rm osc}^2(f, \mathcal{K}) = \sum_{T\in\mathcal{K}} \left\| h_T^2 \left(f - \fint_T f \, dx \right) \right\|_{L^2(T)}^2 \quad \text{for any subset } \mathcal{K} \subseteq \mathcal{T}_\ell.$$

2.4. Adaptive mesh-refinement

Let $\mathcal{T}_0$ be some (coarse) initial triangulation of Ω. The set of regular triangulations created from $\mathcal{T}_0$ by the Newest-Vertex-Bisection (NVB) [24,25] is referred to as set of admissible triangulations and denoted by $\mathbb{T}$.

The adaptive algorithm is driven by this computable error estimator and runs the following loop

Input. Initial triangulation $\mathcal{T}_0$, bulk parameter $0 < \theta \le 1$.
for $\ell = 0, 1, 2, \ldots$ **do**
Solve. Compute discrete solution $u_\ell \in M(\mathcal{T}_\ell)$ of (2.2) with respect to $\mathcal{T}_\ell$.
Estimate. Compute local contributions of the error estimator $\left(\eta_\ell^2(T)\right)_{T\in\mathcal{T}_\ell}$.
Mark. The Dörfler marking chooses a minimal subset $\mathcal{M}_\ell \subseteq \mathcal{T}_\ell$ such that
$\theta \eta_\ell^2(\mathcal{T}_\ell) \le \eta_\ell^2(\mathcal{M}_\ell)$.
Refine. Compute the closure of $\mathcal{M}_\ell$ and generate a new triangulation $\mathcal{T}_{\ell+1}$ using the refinement rules of Fig. 3. **end do**
Output. Sequences of triangulations $(\mathcal{T}_\ell)_\ell$ and finite element solutions $(u_\ell)_\ell$.

3. Discrete Helmholtz decompositions

This section is devoted to the proof of some discrete and continuous Helmholtz-type decompositions. Define

$$\hat{H}^1(\Omega; \mathbb{R}^2) := \left\{ v \in H^1(\Omega; \mathbb{R}^2) \Big| \int_\Omega v \, dx = 0 \text{ and } \int_\Omega {\rm div}\, v \, dx = 0 \right\}$$

and $X(\mathcal{T}_\ell) := P_1(\mathcal{T}; \mathbb{R}^2) \cap \hat{H}^1(\Omega; \mathbb{R}^2)$.

Theorem 3.1 (*Discrete Helmholtz Decomposition for Piecewise Constant Symmetric Tensor Fields*)**.** *Let Ω be simply connected. Given a piecewise constant symmetric tensor field $\sigma_\ell \in P_0(\mathcal{T}_\ell; \mathbb{S})$, there exist unique $\phi_\ell \in M(\mathcal{T}_\ell)$ and $\psi_\ell \in X(\mathcal{T}_\ell)$ such that*

$$\sigma_\ell = D_{\rm NC}^2 \phi_\ell + {\rm sym}\, {\rm Curl}\, \psi_\ell. \tag{3.1}$$

The functions ϕ_ℓ, ψ_ℓ, σ_ℓ from (3.1) satisfy, with the constant $C_{\rm trdevdiv}$ from Lemma 3.3, that

$$|\!|\!| \phi_\ell |\!|\!|_{\rm NC} + \| {\rm Curl}\, \psi_\ell \|_{L^2(\Omega)} \le \max\{1, 3C_{\rm trdevdiv}\} \, \| \sigma_\ell \|_{L^2(\Omega)}. \tag{3.2}$$

The proof is based on an analogue of Korn's inequality. Recall the following well-known result, which is some straightforward modification of [26, Proposition 3.1 in Section IV.3].

Lemma 3.2 (*Tr-Dev-Div Lemma*)**.** *There exists a constant $0 \le C_{\rm trdevdiv} < \infty$ such that any $\rho \in L^2(\Omega; \mathbb{R}^{2\times 2})$ with $\int_\Omega {\rm tr}(\varrho)\, dx = 0$ satisfies*

$$\| \rho \|_{L^2(\Omega;\mathbb{R}^{2\times 2})} \le C_{\rm trdevdiv} (\| {\rm dev}\, \rho \|_{L^2(\Omega;\mathbb{R}^{2\times 2})} + \| {\rm div}\, \rho \|_{H^{-1}(\Omega;\mathbb{R}^2)}). \quad \square$$

Lemma 3.3 (*Korn-Type Inequality*). *Any* $v \in \hat{H}^1(\Omega;\mathbb{R}^2)$ *satisfies*

$$\|\operatorname{Curl} v\|_{L^2(\Omega)} \leq 3C_{\text{trdevdiv}}\,\|\operatorname{sym}\operatorname{Curl} v\|_{L^2(\Omega)}.$$

Proof. Direct calculations in the 2D case reveal

$$\|\operatorname{Curl} v\|_{L^2(\Omega)} = \|Dv\|_{L^2(\Omega)} \quad \text{and} \quad \|\operatorname{sym}\operatorname{Curl} v\|_{L^2(\Omega)} = \|\operatorname{dev} Dv\|_{L^2(\Omega)}. \tag{3.3}$$

Since $\int_\Omega \operatorname{div} v\,dx = 0$, $\rho := Dv$ in Lemma 3.2 leads to

$$\|Dv\|_{L^2(\Omega)} \leq C_{\text{trdevdiv}}\big(\|\operatorname{dev} Dv\|_{L^2(\Omega)} + \|\Delta v\|_{H^{-1}(\Omega)}\big). \tag{3.4}$$

For the estimate of $\|\Delta v\|_{H^{-1}(\Omega)}$, let $\varphi = (\varphi_1;\varphi_2) \in H^1_0(\Omega;\mathbb{R}^2)$ with $\|D\varphi\|_{L^2(\Omega)} = 1$. A direct calculation proves

$$D\varphi + \operatorname{Curl}\begin{pmatrix}\varphi_2\\ -\varphi_1\end{pmatrix} = 2\operatorname{dev}\operatorname{sym} D\varphi.$$

This and the orthogonality of Dv and $\operatorname{Curl}(-\varphi_2;\varphi_1)$ lead to

$$\int_\Omega Dv : D\varphi\,dx = \int_\Omega Dv : \left(D\varphi + \operatorname{Curl}\begin{pmatrix}\varphi_2\\ -\varphi_1\end{pmatrix}\right)dx = 2\int_\Omega Dv : \operatorname{dev}\operatorname{sym} D\varphi\,dx.$$

Since $(\operatorname{dev} A) : B = A : (\operatorname{dev} B)$ for $A, B \in \mathbb{R}^{2\times 2}$, this equals

$$2\int_\Omega \operatorname{dev} Dv : \operatorname{sym} D\varphi\,dx \leq 2\|\operatorname{dev} Dv\|_{L^2(\Omega)}. \tag{3.5}$$

Altogether, this shows

$$\|\Delta v\|_{H^{-1}(\Omega)} \leq 2\|\operatorname{dev} Dv\|_{L^2(\Omega)}.$$

The combination with (3.3)–(3.4) concludes the proof. □

Proof of Theorem 3.1. Since the contributions on the right-hand side of (3.1) are L^2-orthogonal, it suffices to verify that

$$\dim(P_0(\mathcal{T}_\ell;\mathbb{S})) = \dim(D^2_{\text{NC}}(M(\mathcal{T}_\ell))) + \dim(\operatorname{sym}\operatorname{Curl}(X(\mathcal{T}_\ell))). \tag{3.6}$$

Lemma 3.3 implies that the kernel spaces of Curl and sym Curl coincide. Therefore

$$\dim(\operatorname{sym}\operatorname{Curl}(X(\mathcal{T}_\ell))) = \dim(\operatorname{Curl}(X(\mathcal{T}_\ell))) = \dim(D(X(\mathcal{T}_\ell))).$$

Since

$$X(\mathcal{T}_\ell) = \big(P_1(\mathcal{T}_\ell;\mathbb{R}^2)\cap H_1(\Omega;\mathbb{R}^2)\big)\,/\operatorname{span}\left\{\begin{pmatrix}1\\0\end{pmatrix},\begin{pmatrix}0\\1\end{pmatrix},q\right\}$$

for the function $q(\xi) := \xi - \fint_\Omega x\,dx$, the dimension of $D(X(\mathcal{T}_\ell))$ equals $2|\mathcal{N}_\ell| - 3$. Obviously $\dim(P_0(\mathcal{T}_\ell;\mathbb{S})) = 3|\mathcal{T}_\ell|$ and $\dim(D^2_{\text{NC}}(M(\mathcal{T}_\ell))) = |\mathcal{N}_\ell(\Omega)| + |\mathcal{E}_\ell(\Omega)|$. Hence, the proof of (3.6) follows from the well-known Euler formulae

$$|\mathcal{N}_\ell| + |\mathcal{T}_\ell| = 1 + |\mathcal{E}_\ell| \quad \text{and} \quad 2|\mathcal{T}_\ell| + 1 = |\mathcal{N}_\ell| + |\mathcal{E}_\ell(\Omega)|.$$

The proof of the stability (3.2) follows from the orthogonality of the decomposition and Lemma 3.3. □

The following discrete decompositions for general piecewise constant tensor fields are direct consequences of Theorem 3.1.

Corollary 3.4 (*Discrete Helmholtz Decomposition for Piecewise Constant Tensor Fields I*). *Let* Ω *be simply connected. Given a piecewise constant tensor field* $\sigma_\ell \in P_0(\mathcal{T}_\ell;\mathbb{R}^{2\times 2})$, *there exist unique* $\phi_\ell \in M(\mathcal{T}_\ell)$, $\psi_\ell \in X(\mathcal{T}_\ell)$ *and* $\rho_\ell \in P_0(\mathcal{T}_\ell)$ *such that*

$$\sigma_\ell = D^2_{\text{NC}}\phi_\ell + \operatorname{sym}\operatorname{Curl}\psi_\ell + \begin{pmatrix}0 & \rho_\ell\\ -\rho_\ell & 0\end{pmatrix}$$

and

$$|||\phi_\ell|||_{\text{NC}} + \|\operatorname{Curl}\psi_\ell\|_{L^2(\Omega)} + \|\rho_\ell\|_{L^2(\Omega)} \lesssim \|\sigma_\ell\|_{L^2(\Omega)}.$$

Proof. This follows from the orthogonality of the decomposition and the observation that $\dim(P_0(\mathcal{T}_\ell;\mathbb{R}^{2\times 2})) - \dim(P_0(\mathcal{T}_\ell;\mathbb{S})) = |\mathcal{T}_\ell|$. □

Corollary 3.5 (*Discrete Helmholtz Decomposition for Piecewise Constant Tensor Fields II*). *Let* Ω *be simply connected. Given a piecewise constant tensor field* $\sigma_\ell \in P_0(\mathcal{T}_\ell;\mathbb{R}^{2\times 2})$, *there exist* $\phi_\ell \in M(\mathcal{T}_\ell)$, $\psi_\ell \in P_1(\mathcal{T}_\ell;\mathbb{R}^2)\cap H^1(\Omega;\mathbb{R}^2)\cap L^2_0(\Omega;\mathbb{R}^2)$ *and*

$\rho_\ell \in P_0(\mathcal{T}_\ell) \cap L^2_0(\Omega)$ *such that*

$$\sigma_\ell = D^2_{\mathrm{NC}}\phi_\ell + \operatorname{Curl}\psi_\ell + \begin{pmatrix} 0 & \rho_\ell \\ -\rho_\ell & 0 \end{pmatrix}$$

and

$$|||\phi_\ell|||_{\mathrm{NC}} + \|\operatorname{Curl}\psi_\ell\|_{L^2(\Omega)} + \|\rho_\ell\|_{L^2(\Omega)} \lesssim \|\sigma_\ell\|_{L^2(\Omega)}.$$

Proof. The fact that, for any $\vartheta \in H^1(\Omega;\mathbb{R}^2)$,

$$\operatorname{Curl}\vartheta = \operatorname{sym}\operatorname{Curl}\vartheta + \begin{pmatrix} 0 & \operatorname{div}\vartheta \\ -\operatorname{div}\vartheta & 0 \end{pmatrix} \quad \text{and} \quad \begin{pmatrix} 0 & 1 \\ -1 & 0 \end{pmatrix} = \operatorname{Curl} q \tag{3.7}$$

for the function $q(\xi) := \xi - \fint_\Omega x\,dx$ and Corollary 3.4 imply the assertion. □

The decomposition of Corollary 3.5 is a discrete analogue of [8, Lemma 1]. It allows for an alternative proof of that result. Recall that Ω is simply connected.

Theorem 3.6 (*Lemma 1 of [8]*)**.** *Given any $\sigma \in L^2(\Omega;\mathbb{R}^{2\times 2})$, there exist $\phi \in H^2_0(\Omega)$, $\psi \in H^1(\Omega;\mathbb{R}^2) \cap L^2_0(\Omega;\mathbb{R}^2)$ and $\rho \in L^2_0(\Omega)$ such that*

$$\sigma = D^2\phi + \operatorname{Curl}\psi + \begin{pmatrix} 0 & \rho \\ -\rho & 0 \end{pmatrix}$$

and

$$\|D^2\phi\|_{L^2(\Omega)} + \|\operatorname{Curl}\psi\|_{L^2(\Omega)} + \|\rho\|_{L^2(\Omega)} \lesssim \|\sigma\|_{L^2(\Omega)}.$$

Proof. Let $(\mathcal{T}_\ell \mid \ell \in \mathbb{N})$ denote a sequence of uniformly refined triangulations of Ω and let $\sigma_\ell := \Pi_{0,\ell}\sigma$. Corollary 3.4 yields

$$\sigma_\ell = D^2_{\mathrm{NC}}\phi_\ell + \operatorname{sym}\operatorname{Curl}\psi_\ell + \begin{pmatrix} 0 & \rho_\ell \\ -\rho_\ell & 0 \end{pmatrix}.$$

The stability of the decomposition shows that there exists a subsequence (not relabeled here for simplicity) such that, for $\ell \to \infty$,

$$D^2_{\mathrm{NC}}\phi_\ell \rightharpoonup A, \qquad \operatorname{sym}\operatorname{Curl}\psi_\ell \rightharpoonup B, \qquad \rho_\ell \rightharpoonup \tilde{\rho} \quad \text{in } L^2(\Omega;\mathbb{R}^{2\times 2}) \text{ or } L^2(\Omega). \tag{3.8}$$

Let $m \geq n \geq \ell$. The fact that $\operatorname{sym}\operatorname{Curl}\psi_{\ell+n} \in P_0(\mathcal{T}_{\ell+n};\mathbb{R}^{2\times 2}) \subseteq P_0(\mathcal{T}_{\ell+m};\mathbb{R}^{2\times 2})$ and the orthogonality of the decomposition prove

$$\begin{aligned}\int_\Omega \sigma : \operatorname{sym}\operatorname{Curl}\psi_{\ell+n}\,dx &= \int_\Omega \sigma_{\ell+m} : \operatorname{sym}\operatorname{Curl}\psi_{\ell+n}\,dx \\ &= \int_\Omega \operatorname{sym}\operatorname{Curl}\psi_{\ell+m} : \operatorname{sym}\operatorname{Curl}\psi_{\ell+n}\,dx.\end{aligned}$$

Hence,

$$\|\operatorname{sym}\operatorname{Curl}(\psi_{\ell+m} - \psi_{\ell+n})\|^2_{L^2(\Omega)} = \int_\Omega \sigma : \operatorname{sym}\operatorname{Curl}(\psi_{\ell+m} - \psi_{\ell+n})\,dx \to 0 \quad \text{as } m, n \to \infty.$$

This and analogous arguments for the remaining contributions show that the convergence in (3.8) is indeed strongly in $L^2(\Omega)$ or $L^2(\Omega;\mathbb{R}^{2\times 2})$. Therefore, $B = \operatorname{sym}\operatorname{Curl}\tilde{\psi}$ for some $\tilde{\psi} \in \hat{H}^1(\Omega;\mathbb{R}^2)$ and $\tilde{\rho} \in L^2(\Omega)$. For the proof that $A = D^2\phi$ for some $\phi \in H^2_0(\Omega)$, let $\varphi : \Omega \to \mathbb{R}^{2\times 2}$ be a smooth test function. The integration by parts reveals, for any $\ell \in \mathbb{N}$, that

$$\int_\Omega D^2_{\mathrm{NC}}\phi_\ell : \varphi\,dx = \sum_{E\in\mathcal{E}_\ell}\left(\int_E [\nabla_{\mathrm{NC}}\phi_\ell]_E \cdot \nu_E\varphi\,ds - \int_E [\phi_\ell]_E \operatorname{div}\varphi\cdot\nu_E\,ds\right) + \int_\Omega \phi_\ell : \operatorname{div}\operatorname{div}\varphi\,dx,$$

where the divergence of a vector field is understood row-wise. For any edge $E \in \mathcal{E}_\ell$, the Poincaré and Friedrichs inequalities and the trace inequality prove that

$$\|[\nabla_{\mathrm{NC}}\phi_\ell]_E\|_{L^2(E)} \lesssim h_E^{1/2}\|D^2_{\mathrm{NC}}\phi_\ell\|_{L^2(\omega_E)} \quad \text{and} \quad \|[\phi_\ell]_E\|_{L^2(E)} \lesssim h_E^{3/2}\|D^2_{\mathrm{NC}}\phi_\ell\|_{L^2(\omega_E)}.$$

Hence, the jump contributions vanish in the limit $\ell \to \infty$. The Friedrichs inequality shows $\phi_\ell \rightharpoonup \phi \in L^2(\Omega)$ and so

$$\int_\Omega A : \varphi\,dx = \lim_{\ell\to\infty}\int_\Omega D^2_{\mathrm{NC}}\phi_\ell : \varphi\,dx = \lim_{\ell\to\infty}\int_\Omega \phi_\ell \operatorname{div}\operatorname{div}\varphi\,dx = \int_\Omega \phi \operatorname{div}\operatorname{div}\varphi\,dx.$$

Therefore, $A = D^2\phi$ and $\phi \in H^2_0(\Omega)$. This establishes the decomposition

$$\sigma = D^2\phi + \operatorname{sym}\operatorname{Curl}\tilde{\psi} + \begin{pmatrix} 0 & \tilde{\rho} \\ -\tilde{\rho} & 0 \end{pmatrix}$$

and

$$\|D^2\phi\|_{L^2(\Omega)} + \|\operatorname{Curl}\tilde{\psi}\|_{L^2(\Omega)} + \|\tilde{\rho}\|_{L^2(\Omega)} \lesssim \|\sigma\|_{L^2(\Omega)}.$$

Define the functions $\psi \in H^1(\Omega;\mathbb{R}^2) \cap L^2_0(\Omega;\mathbb{R}^2)$ and $\rho \in L^2_0(\Omega)$ via

$$\psi(\xi) := \tilde{\psi}(\xi) + \fint_\Omega \tilde{\rho}\,dx \left(\xi - \fint_\Omega x\,dx\right) \quad \text{and} \quad \rho := \tilde{\rho} - \fint_\Omega \tilde{\rho}\,dx - \operatorname{div}\tilde{\psi}.$$

The observation (3.7) proves the asserted decomposition. The stability follows from the triangle inequality. □

4. Discrete reliability

This section is devoted to the proof of discrete reliability via the discrete Helmholtz-type decomposition of Section 3. This is an alternative approach to [11, Lemma 5.5].

Theorem 4.1 (*Discrete Reliability*)**.** *There exists a constant $C_{\mathrm{drel}} \approx 1$ such that any admissible refinement $\mathcal{T}_{\ell+m} \in \mathbb{T}$ of $\mathcal{T}_\ell \in \mathbb{T}$ and the respective discrete solutions $u_\ell \in M(\mathcal{T}_\ell)$ and $u_{\ell+m} \in M(\mathcal{T}_{\ell+m})$ satisfy*

$$|||u_\ell - u_{\ell+m}|||^2_{\mathrm{NC}} \le C_{\mathrm{drel}}\eta_\ell(\mathcal{T}_\ell \setminus \mathcal{T}_{\ell+m})^2.$$

Proof. The discrete Helmholtz decomposition from Theorem 3.1 leads to $\phi_{\ell+m} \in M(\mathcal{T}_{\ell+m})$ and $\psi_{\ell+m} \in X(\mathcal{T}_{\ell+m})$ such that

$$D^2_{\mathrm{NC}}(u_{\ell+m} - u_\ell) = D^2_{\mathrm{NC}}\phi_{\ell+m} + \operatorname{sym}\operatorname{Curl}\psi_{\ell+m}.$$

The orthogonality of the decomposition proves

$$|||u_{\ell+m} - u_\ell|||^2_{\mathrm{NC}} = a_{\mathrm{NC}}(u_{\ell+m} - u_\ell, \phi_{\ell+m}) - \int_\Omega D^2_{\mathrm{NC}}u_\ell : \operatorname{Curl}\psi_{\ell+m}\,dx. \tag{4.1}$$

The Morley interpolation operator $I_\ell : M(\mathcal{T}_{\ell+m}) \to M(\mathcal{T}_\ell)$ is defined via

$$(I_\ell v_{\ell+m})(z) = v_{\ell+m}(z) \quad \text{for any } z \in \mathcal{N}_\ell \text{ and any } v_{\ell+m} \in M(\mathcal{T}_{\ell+m})$$
$$\int_E \frac{\partial I_\ell v_{\ell+m}}{\partial \nu_E}\,ds = \int_E \frac{\partial v_{\ell+m}}{\partial \nu_E}\,ds \quad \text{for any } E \in \mathcal{E}_\ell \text{ and any } v_{\ell+m} \in M(\mathcal{T}_{\ell+m})$$

and satisfies the following approximation and stability property [11] for any $T \in \mathcal{T}_\ell$

$$\|h_T^{-2}(1 - I_\ell)v_{\ell+m}\|_{L^2(T)} + \|h_T^{-1}\nabla_{\mathrm{NC}}(1 - I_\ell)v_{\ell+m}\|_{L^2(T)} + \|D^2_{\mathrm{NC}}I_\ell v_{\ell+m}\|_{L^2(T)} \lesssim \|D^2_{\mathrm{NC}}v_{\ell+m}\|_{L^2(T)}. \tag{4.2}$$

A piecewise integration by parts proves the projection property

$$\Pi_{0,\ell}D^2_{\mathrm{NC}} = D^2_{\mathrm{NC}}I_\ell. \tag{4.3}$$

The projection property of the Morley interpolation operator (4.3) and the approximation and stability property (4.2) prove for the first term of (4.1) that

$$a_{\mathrm{NC}}(u_{\ell+m} - u_\ell, \phi_{\ell+m}) = \int_\Omega f(1 - I_\ell)\phi_{\ell+m}\,dx \lesssim \|h_\ell^2 f\|_{L^2(\cup(\mathcal{T}_\ell \setminus \mathcal{T}_{\ell+m}))}|||\phi_{\ell+m}|||_{\mathrm{NC}}.$$

Let $\psi_\ell \in P_1(\mathcal{T}_\ell) \cap H^1(\Omega)$ denote the Scott–Zhang quasi-interpolation [27] of $\psi_{\ell+m}$ with the property that $\psi_\ell|_E = \psi_{\ell+m}|_E$ for all edges $E \in \mathcal{E}_\ell \cap \mathcal{E}_{\ell+m}$. Since $\operatorname{Curl}\psi_\ell$ and $D^2_{\mathrm{NC}}u_\ell$ are L^2-orthogonal, an integration by parts shows for the second term of (4.1)

$$\int_\Omega D^2_{\mathrm{NC}}u_\ell : \operatorname{Curl}\psi_{\ell+m}\,dx = \sum_{E \in \mathcal{E}_\ell \setminus \mathcal{E}_{\ell+m}} \int_E ([D^2_{\mathrm{NC}}u_\ell]_E\tau_E) \cdot (\psi_{\ell+m} - \psi_\ell)\,ds.$$

Cauchy and trace inequalities and the approximation and stability properties of the Scott–Zhang quasi-interpolation prove that this is bounded by

$$\left(\sum_{T \in \mathcal{T}_\ell \setminus \mathcal{T}_{\ell+m}} \sum_{E \in \mathcal{E}(T)} h_E\|[D^2_{\mathrm{NC}}u_\ell]_E\tau_E\|^2_{L^2(E)}\right)^{1/2} \|D\psi_{\ell+m}\|_{L^2(\Omega)}.$$

The combination of the foregoing estimates and the stability (3.2) conclude the proof. □

5. Optimal convergence rates

This section outlines the proof of Theorem 5.1 (Theorem 6.2 from [11]) and follows the standard arguments from [13,25], cf. also [14] for a more general paradigm of optimality of adaptive algorithms. This outline is added for completeness and a convenient reading to underline the role of discrete reliability.

5.1. Approximation classes and optimality result

Let, for any $N \in \mathbb{N}$,

$$\mathbb{T}(N) := \{\mathcal{T} \in \mathbb{T} \mid |\mathcal{T}| - |\mathcal{T}_0| \leq N\}$$

and define the seminorm

$$|(u,f)|_{\mathcal{A}_s} := \sup_{N\in\mathbb{N}} N^s \inf_{\mathcal{T}\in\mathbb{T}(N)} \left(\|(1-\Pi_{0,\mathcal{T}})D^2u\|^2_{L^2(\Omega)} + \operatorname{osc}^2(f,\mathcal{T})\right)^{1/2}$$

and the approximation class

$$\mathcal{A}_s := \left\{(u,f) \in V \times L^2(\Omega) \middle| \, |(u,f)|_{\mathcal{A}_s} \leq \infty\right\}.$$

An alternative approximation class reads

$$\mathcal{A}'_s := \left\{(u,f) \in V \times L^2(\Omega) \middle| \, \Delta^2 u = f \text{ in } H^{-2}(\Omega) \text{ and } |(u,f)|_{\mathcal{A}'_s} \leq \infty\right\}$$

for the seminorm

$$|(u,f)|_{\mathcal{A}'_s} := \sup_{N\in\mathbb{N}} N^s \left(\inf_{\mathcal{T}\in\mathbb{T}(N)} |||u - u_{\mathcal{T}}|||^2_{\mathrm{NC}} + \operatorname{osc}^2(f,\mathcal{T})\right)^{1/2}$$

where $u_{\mathcal{T}}$ is the Morley FEM solution of (2.2) with respect to $\mathcal{T}$ and the right-hand side f.

The best-approximation results of [7, Lemma 2.1] show that

$$|||u - u_{\mathcal{T}}|||^2_{\mathrm{NC}} \lesssim \|(1-\Pi_{0,\mathcal{T}})D^2u\|^2_{L^2(\Omega)} + \operatorname{osc}^2(f,\mathcal{T}).$$

Therefore the approximation classes are equivalent in the sense that

$$(u, \Delta^2 u) \in \mathcal{A}_s \quad \text{if and only if} \quad (u, \Delta^2 u) \in \mathcal{A}'_s.$$

The optimality result is stated in the following theorem.

Theorem 5.1 (*Optimal Convergence Rates*)**.** *Let Ω be simply connected. For any $(u, \Delta^2 u) \in \mathcal{A}_s$, the adaptive algorithm of Section 2.4 computes sequences of triangulations $(\mathcal{T}_\ell)_\ell$ and discrete Morley FEM solutions $(u_\ell)_\ell$ with optimal rate of convergence in the sense that for sufficiently small $\theta \ll 1$ there exists a constant $C_{\mathrm{opt}} \approx 1$ such that*

$$(|\mathcal{T}_\ell| - |\mathcal{T}_0|)^s \sqrt{|||u - u_\ell|||^2_{\mathrm{NC}} + \operatorname{osc}^2(f,\mathcal{T}_\ell)} \leq C_{\mathrm{opt}} |(u, \Delta^2 u)|_{\mathcal{A}_s}.$$

The proof follows in Section 5.2 and employs the following two results of [11].

Theorem 5.2 (*Quasi-Orthogonality, Lemma 3.4 of [11]*)**.** *Let $\mathcal{T}_{\ell+m} \in \mathbb{T}$ be some admissible refinement of $\mathcal{T}_\ell \in \mathbb{T}$. The discrete solutions $u_\ell \in M(\mathcal{T}_\ell)$ and $u_{\ell+m} \in M(\mathcal{T}_{\ell+m})$ satisfy for a constant $C_{\mathrm{qo}} \approx 1$ that*

$$|a_{\mathrm{NC}}(u - u_{\ell+m}, u_{\ell+m} - u_\ell)| \leq C_{\mathrm{qo}} \sum_{T\in\mathcal{T}_\ell\setminus\mathcal{T}_{\ell+m}} \|h^2_{\mathcal{T}} f\|_{L^2(T)} \|D^2_{\mathrm{NC}}(u - u_{\ell+m})\|_{L^2(T)}. \quad \square$$

Theorem 5.3 (*Contraction Property, Theorem 4.5 of [11]*)**.** *There exist constants $0 < \rho < 1$ and $0 < \beta, \gamma < \infty$ such that for $\mathcal{T}_\ell$ and its one-level refinement $\mathcal{T}_{\ell+1}$ created by AFEM, the quantity*

$$\xi^2_\ell := |||u - u_\ell|||^2_{\mathrm{NC}} + \beta \|h^2_\ell f\|^2_{L^2(\Omega)} + \gamma \eta^2_\ell$$

contracts in the sense that

$$\xi_{\ell+1} \leq \rho \xi_\ell \quad \text{for all } \ell = 0, 1, 2, \ldots. \quad \square$$

5.2. Proof of optimality

This subsection outlines the optimality proof of [11]. Let, for any $\ell \in \mathbb{N}$, $e^2_\ell := |||u - u_\ell|||^2_{\mathrm{NC}} + \operatorname{osc}^2(f,\mathcal{T}_\ell)$. The optimality proof makes use of the following consequence of the quasi-orthogonality (Theorem 5.2) and the efficiency of the error estimator. There exists a constant $C \approx 1$ such that for $\mathcal{T}_\ell$ and any refinement $\mathcal{T}_{\ell+m} \in \mathbb{T}$ there holds

$$e^2_{\ell+m} \leq C e^2_\ell. \tag{5.1}$$

Lemma 5.4 (*Lemma 6.1 of [11]*). *For any $\ell \in \mathbb{N}$ the number of marked triangles is controlled as*

$$|\mathcal{M}_\ell| \lesssim |(u,f)|_{\mathcal{A}_s}^{1/s}\, e_\ell^{-1/s}.$$

Proof. Let $0 < \alpha < 1$ and $\epsilon^2 := C^{-1}\alpha e_\ell^2$. Since $(u,f) \in \mathcal{A}_s'$, there exists an optimal triangulation $\mathcal{T}_\epsilon \in \mathbb{T}$ with Morley finite element solution $u_\epsilon \in M(\mathcal{T}_\epsilon)$ such that

$$|\mathcal{T}_\epsilon| - |\mathcal{T}_0| \le |(u,f)|_{\mathcal{A}_s'}^{1/s}\epsilon^{-1/s} \quad \text{and} \quad |||u-u_\epsilon|||_{\mathrm{NC}}^2 + \mathrm{osc}^2(f,\mathcal{T}_\epsilon) \le \epsilon^2. \tag{5.2}$$

Let $\mathcal{T}_\star$ denote the overlay of $\mathcal{T}_\ell$ and $\mathcal{T}_\epsilon$ defined as the smallest common refinement of $\mathcal{T}_\ell$ and $\mathcal{T}_\epsilon$ and let $u_\star$ denote the discrete FEM solution with respect to $\mathcal{T}_\star$. The estimate (5.1) proves

$$|||u-u_\star|||_{\mathrm{NC}}^2 + \mathrm{osc}^2(f,\mathcal{T}_\star) \le C\epsilon^2 = \alpha e_\ell^2.$$

The quasi-orthogonality from Theorem 5.2 followed by the Young inequality prove

$$|2a_{\mathrm{NC}}(u-u_\star, u_\star - u_\ell)| \le \frac{(1-\alpha)}{2}e_\ell^2 + 2C_{\mathrm{qo}}^2\frac{\alpha}{1-\alpha}\eta_\ell^2(u_\ell, \mathcal{T}_\ell\setminus\mathcal{T}_\star).$$

The foregoing two displayed estimates together with the definition of ϵ and the discrete reliability from Theorem 4.1 prove

$$\begin{aligned}(1-\alpha)e_\ell^2 &\le |||u_\ell - u_\star|||_{\mathrm{NC}}^2 + 2a_{\mathrm{NC}}(u-u_\star, u_\star-u_\ell) + \mathrm{osc}^2(f,\mathcal{T}_\ell) - \mathrm{osc}^2(f,\mathcal{T}_\star)\\ &\le \frac{(1-\alpha)}{2}e_\ell^2 + \left(1 + 2C_{\mathrm{qo}}^2\frac{\alpha}{1-\alpha} + C_{\mathrm{drel}}\right)\eta_\ell^2(\mathcal{T}_\ell\setminus\mathcal{T}_\star).\end{aligned}$$

Thus, the efficiency $\eta_\ell^2 \le C_{\mathrm{eff}}\, e_\ell^2$ leads to

$$\theta\eta_\ell^2(\mathcal{T}_\ell) \le \eta_\ell^2(\mathcal{T}_\ell\setminus\mathcal{T}_\star)$$

for $\theta < (1-\alpha)^2/\big(2C_{\mathrm{eff}}((1-\alpha)(1+C_{\mathrm{drel}}) + 2\alpha C_{\mathrm{qo}}^2)\big)$. Hence, $\mathcal{T}_\ell\setminus\mathcal{T}_\star$ satisfies the bulk criterion. The minimality of $\mathcal{M}_\ell$ and the properties of the overlay prove

$$|\mathcal{M}_\ell| \le |\mathcal{T}_\star| - |\mathcal{T}_\ell| \le |\mathcal{T}_\epsilon| - |\mathcal{T}_0|.$$

This and (5.2) conclude the proof. □

Proof of Theorem 5.1. The contraction from Theorem 5.3 and the reliability and efficiency (2.3) prove for any $k \in \mathbb{N}$ with $k \le \ell$ that

$$e_\ell \lesssim \xi_\ell \lesssim \rho^k e_{\ell-k}.$$

The overhead control $|\mathcal{T}_\ell| - |\mathcal{T}_0| \lesssim \sum_{j=1}^{\ell}|\mathcal{M}_j|$ from [24], Lemma 5.4 and (5.1) therefore lead to

$$|\mathcal{T}_\ell| - |\mathcal{T}_0| \lesssim \sum_{j=1}^{\ell}|\mathcal{M}_j| \lesssim |(u,f)|_{\mathcal{A}_s'}^{1/s}\, e_\ell^{-1/s}\sum_{k=1}^{\ell}\rho^{(\ell-k)/s}.$$

Since the geometric sum on the right-hand side is uniformly bounded, the equivalence of $|(u,f)|_{\mathcal{A}_s'}$ and $|(u,f)|_{\mathcal{A}_s}$ concludes the proof. □

6. Numerical realization

This section introduces a Matlab program to compute the Morley FEM solution of $\Delta^2 u = f$ with clamped boundary conditions in the spirit of [28].

6.1. Shape functions

The three vertices of the triangle T are denoted by P_1, P_2, P_3 and the edges opposite are denoted by E_1, E_2, E_3 as depicted in Fig. 4. Each edge E_j is equipped with a global sign $\sigma_j \in \{\pm 1\}$ such that $\nu_{E_j} = \sigma_j \nu_T$. Let $\varphi_1, \varphi_2, \varphi_3$ denote the barycentric coordinates on T. The six local basis functions [29] read

$$\begin{aligned}\psi_j &= \varphi_j + 2\varphi_{j+1}\varphi_{j-1} - \nabla\varphi_{j+1}\cdot\nabla\varphi_{j-1}\sum_{k\neq j}\varphi_k(\varphi_k-1)/|\nabla\varphi_k|^2,\\ \psi_{3+j} &= \sigma_j\varphi_j(\varphi_j-1)/|\nabla\varphi_j| \quad \text{for } j = 1,2,3\end{aligned} \tag{6.1}$$

and satisfy (with the Kronecker δ) that for all $j, k = 1, 2, 3$

$$\psi_j(P_k) = \frac{\partial\psi_{3+j}}{\partial\nu_E}(\mathrm{mid}(E_k)) = \delta_{jk} \quad \text{and} \quad \psi_{3+j}(P_k) = \frac{\partial\psi_j}{\partial\nu_E}(\mathrm{mid}(E_k)) = 0.$$

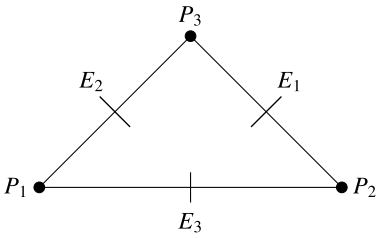

Fig. 4. Local enumeration of vertices and edges.

6.2. Local stiffness matrix

The second derivatives of ψ_1, ψ_2, ψ_3 read

$$\frac{\partial^2 \psi_j}{\partial x_k \partial x_\ell} = \begin{bmatrix} \frac{\partial \varphi_{j+1}}{\partial x_k} & \frac{\partial \varphi_{j-1}}{\partial x_\ell} \end{bmatrix} \begin{bmatrix} -2\frac{\nabla \varphi_{j+1} \cdot \nabla \varphi_{j-1}}{|\nabla \varphi_{j-1}|^2} & 2 \\ 2 & -2\frac{\nabla \varphi_{j+1} \cdot \nabla \varphi_{j-1}}{|\nabla \varphi_{j-1}|^2} \end{bmatrix} \begin{bmatrix} \frac{\partial \varphi_{j+1}}{\partial x_k} \\ \frac{\partial \varphi_{j-1}}{\partial x_\ell} \end{bmatrix}.$$

With the matrices

$$G := \begin{bmatrix} \partial\varphi_1/\partial x_1 & \partial\varphi_1/\partial x_2 \\ \partial\varphi_2/\partial x_1 & \partial\varphi_2/\partial x_2 \\ \partial\varphi_3/\partial x_1 & \partial\varphi_3/\partial x_2 \end{bmatrix} \quad \text{and} \quad M := G^\top G = \left(\nabla\varphi_j \cdot \nabla\varphi_k\right)_{j,k=1,2,3},$$

the first three rows of the Hessians `H(1:3,:)` are computed as a result of the lines 16–19 in the program displayed in Section 6.5. The second derivatives of ψ_4, ψ_5, ψ_6 read

$$\frac{\partial^2 \psi_{j+3}}{\partial x_k \partial x_\ell} = \frac{2\,\sigma_j}{|\nabla \varphi_j|} \frac{\partial \varphi_j}{\partial x_k} \frac{\partial \varphi_j}{\partial x_\ell} \quad \text{for } j = 1, 2, 3;\ k, \ell = 1, 2.$$

The Hessians `H(4:6,:)` are computed by line 19 in Section 6.5. This leads to the local stiffness matrix

$$STIMA(T) := \left(\int_T D^2\psi_j : D^2\psi_k \, dx \right)_{j,k=1,\ldots,6} = |T|\, H\, \mathrm{diag}(1, 2, 1)\, H^\top.$$

6.3. Right-hand side

For any T, the contribution to the right-hand side vector is computed with the quadrature formula which is exact for piecewise constant f,

$$\int_T f\,\psi_j \, dx = \frac{1}{3} \sum_{j=1}^{3} f(\mathrm{mid}(E_j))\, \psi_j(\mathrm{mid}(E_j)).$$

The evaluation of $\psi_1, \ldots, \psi_3$ at the quadrature points is realized in line 21 while $\psi_4, \ldots, \psi_6$ are evaluated in line 22 of the program in Section 6.5. The resulting matrix

$$Q := \left[\psi_j(\mathrm{mid}(E_k)) \big|_{k=1,\ldots,3}^{j=1,\ldots,6} \right]$$

is used in line 23 to perform the quadrature

$$\int_T f \begin{bmatrix} \psi_1 \\ \vdots \\ \psi_6 \end{bmatrix} dx = \frac{|T|}{3} Q^\top \begin{bmatrix} f(\mathrm{mid}(E_1)) \\ f(\mathrm{mid}(E_2)) \\ f(\mathrm{mid}(E_3)) \end{bmatrix}.$$

6.4. Data structures

The triangulation $\mathcal{T}$ is described by the matrices `c4n` $\in \mathbb{R}^{|N|\times 2}$ and `n4e` $\in \mathbb{R}^{|T|\times 3}$ where the jth row of `c4n` contains the coordinates of the vertex z_j while the jth row of `n4e` gives the global numbers of the vertices of the triangle T_j. The rows of `n4sCb` $\in \mathbb{R}^{|\mathcal{E}(\partial\Omega)|\times 2}$ contain the numbers of the two endpoints of the boundary edges. The global edge enumeration `n4s` is computed from the input in line 4. For the edge $E_j = \mathrm{conv}\{z_k, z_\ell\}$, the entry reads `n4s(j,:)` $= [\mathtt{k}, \ell]$. The three edge numbers of each triangle are described by the rows of `s4e`. If the nodes with global numbers `j`, `k` are the endpoints of the edge number ℓ, then sparse matrix `s4n` has the entry `s4n(j,k)` $= \ell$ and zero otherwise. Finally, each row of `e4s` $\in \mathbb{R}^{|\mathcal{E}|\times 2}$ gives the numbers of the triangles T_+, T_- shared by an edge E. For edges on the boundary, the second entry is zero.

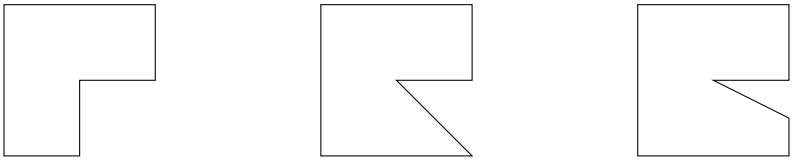

Fig. 5. L-shaped domain, domain with 1/8 cusp and domain with 1/16 cusp.

6.5. Matlab program

The assembly and overall setting of the program is rather standard [28,30] and not further discussed in this paper because the complete script fits into 30 lines of Matlab. Given the geometry `c4n`, `n4e`, the boundary data `n4sCb` and the load function `f` as input as described in Section 6.4, the following function computes the Morley FEM approximation of the biharmonic problem.

```
function x = MorleyFEM(c4n,n4e,n4sCb,f)
allSides = [n4e(:,[2 3]); n4e(:,[3 1]); n4e(:,[1 2])];
[~,ind,back] = unique(sort(allSides,2),'rows');
n4s = allSides(ind,:);   s4e = reshape(back,size(n4e));
s4n = sparse(n4s(:,1),n4s(:,2),1:size(n4s,1),size(c4n,1),size(c4n,1));
s4n = s4n + s4n';                    ElemNrs = repmat(1:size(n4e,1),1,3);
allElem4s(ind)=accumarray(back,ElemNrs);
e4s = [ElemNrs(ind)', allElem4s(ind)'-ElemNrs(ind)'];
A = sparse(size(c4n,1)+size(n4s,1),size(c4n,1)+size(n4s,1));
b=zeros(size(A,1),1);       x=b;    I=[2,3,3,1,1,2];
for el = 1 : size(n4e,1) % loop over all triangles
L=[n4e(el,:),size(c4n,1)+s4e(el,:)];
area = det([1,1,1;c4n(L(1:3),:)'])/2;  sg=[1;1;1]-2*(e4s(s4e(el,:),2)==el);
G = [1,1,1;c4n(L(1:3),:)'] \ [0,0;eye(2)];     M  = G*G';   z=diag(M);
R = repmat([M(2,3);M(3,1);M(1,2)],1,2)./[z([2,3,1]),z([3,1,2])];
H=[reshape(G([I,3+I,3+I])*...
   (kron(eye(9),[0,2;2,0])-2*diag(repmat(reshape(R',1,6),1,3)))*...
   blkdiag(G(2:3),G([3,1]),G(1:2),G(2:3),G([3,1]),G(1:2),G(5:6),...
   G([6,4]),G(4:5))',3,3);2*diag(sg./sqrt(z))*G(:,[1,2,2]).*G(:,[1,1,2])];
A(L,L) = A(L,L)+ area*H*diag([1,2,1])*H';
Q=[.5+([0,R([2,3],2)';R(1,2),0,R(3,2);R(3,[2,1]),0]+diag(sum(R,2)))/4,...
   repmat(sg'./sqrt(z)',3,1).*(ones(3)-eye(3))/9];
b(L)=b(L)+area/3 *Q'*(f((c4n(L(1:3),:)+c4n(L([2,3,1]),:))/2)); end
CbSides = s4n((n4sCb(:,1)-1)*size(c4n,1)+n4sCb(:,2));
dof = setdiff(1:size(A,1),[unique(n4sCb);size(c4n,1)+CbSides]);
x(dof) = A(dof,dof)\b(dof);
```

The solution can be plotted with the following lines

```
X=c4n(:,1)'; Y=c4n(:,2)'; Xcrd=X(n4e)'; Ycrd=Y(n4e)';
Z=x(n4e)'; C=sum(Z,1)/3; figure; patch(Xcrd,Ycrd,Z,C); view(-37.5,30);
```

Remark 6.1. The update of the sparse matrix in each loop iteration can be replaced by building the stiffness matrix directly from an array of local stiffness matrices and proper index sets as described in [31].

7. Numerical examples

This section presents numerical tests on the performance of the adaptive Morley FEM and illustrates the optimal convergence rates as well as the superiority of adaptive over uniform mesh-refinement.

7.1. Realization

The computational tests are carried out for the three nonconvex domains of Fig. 5. The convergence history plots compare the convergence rates for bulk parameters $\theta = 0.1, \ldots, 0.9$ with uniform mesh-refinement.

The error quantities in the convergence history plots are plotted against the degrees of freedom. Besides η_ℓ and $|||u-u_\ell|||_{\mathrm{NC}}$, the averaging error estimator of [32] is plotted for comparison. Define the piecewise affine H^1 tensor field $\sigma_{\mathrm{av},\ell}$ by

$$\sigma_{\mathrm{av},\ell}(z) := \fint_{\omega_z} D^2_{\mathrm{NC}} u_\ell \, dx \quad \text{for any } z \in \mathcal{N}$$

for the nodal patch $\omega_z = \cup\{T \in \mathcal{T}_\ell \mid z \in T\}$. The reliability

$$|||u - u_\ell|||_{\mathrm{NC}} \lesssim \|D^2_{\mathrm{NC}} u_\ell - \sigma_{\mathrm{av},\ell}\|_{L^2(\Omega)} + \|h^2_\ell f\|_{L^2(\Omega)}$$

is proven in [32].

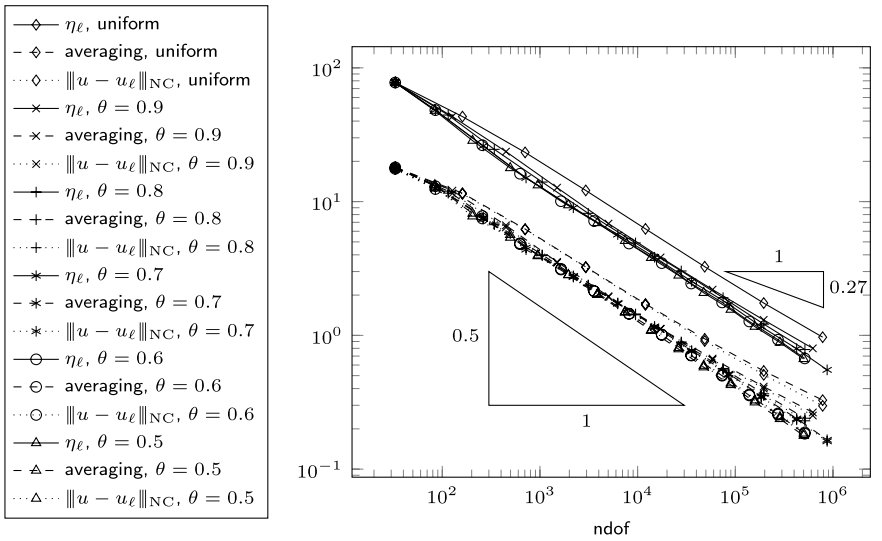

Fig. 6. Convergence history of the error and estimators for the L-shaped domain with $\theta = 0.5, \ldots, 0.9$ and uniform mesh-refinement.

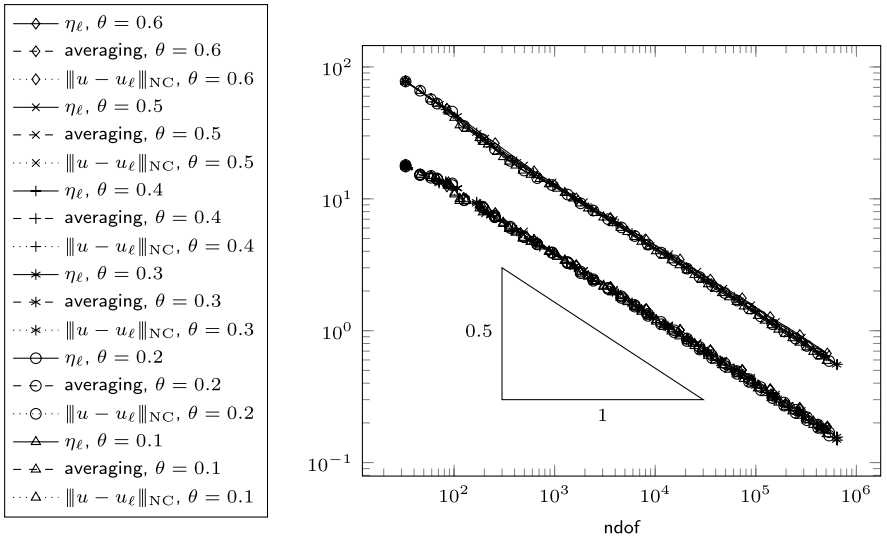

Fig. 7. Convergence history of the error and estimators for the L-shaped domain with $\theta = 0.1, \ldots, 0.6$.

7.2. L-shaped domain

Consider the L-shaped domain $\Omega = (-1, 1)^2 \setminus ([0, 1] \times [-1, 0])$ with $\alpha := 0.5444837$ and $\omega := 3\pi/2$. The exact singular solution from [33, p. 107] reads in polar coordinates as

$$u(r, \theta) = (r^2 \cos^2\theta - 1)^2 \, (r^2 \sin^2\theta - 1)^2 \, r^{1+\alpha} \, g_{\alpha,\omega}(\theta) \tag{7.1}$$

for

$$g_{\alpha,\omega}(\theta) = \left(\frac{1}{\alpha - 1}\sin((\alpha - 1)\omega) - \frac{1}{\alpha + 1}\sin((\alpha + 1)\omega)\right)\big(\cos((\alpha - 1)\theta) - \cos((\alpha + 1)\theta)\big)$$
$$- \left(\frac{1}{\alpha - 1}\sin((\alpha - 1)\theta) - \frac{1}{\alpha + 1}\sin((\alpha + 1)\theta)\right)\big(\cos((\alpha - 1)\omega) - \cos((\alpha + 1)\omega)\big).$$

Figs. 6–7 show the convergence history of the error estimators and the exact error for uniform and adaptive meshes. The convergence rates for uniform mesh-refinement as well as for large values of θ is sub-optimal. The choice of $\theta \leq 0.5$ leads to the optimal convergence rate starting from the first loop in the adaptive algorithm. The averaging error estimator is very accurate in the sense that both the reliability and efficiency constants seem to be close to 1.

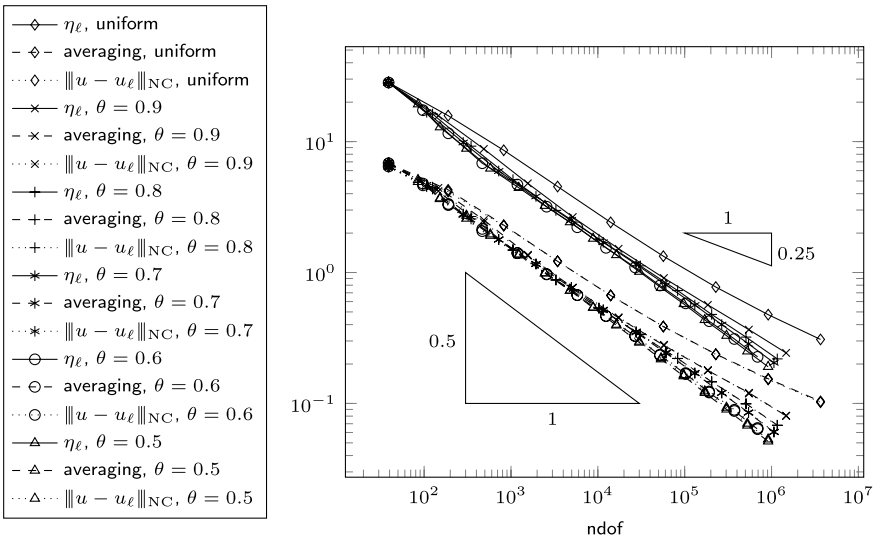

Fig. 8. Convergence history of the error and estimators for the 1/8 cusp domain with $\theta = 0.5, \ldots, 0.9$ and uniform mesh-refinement.

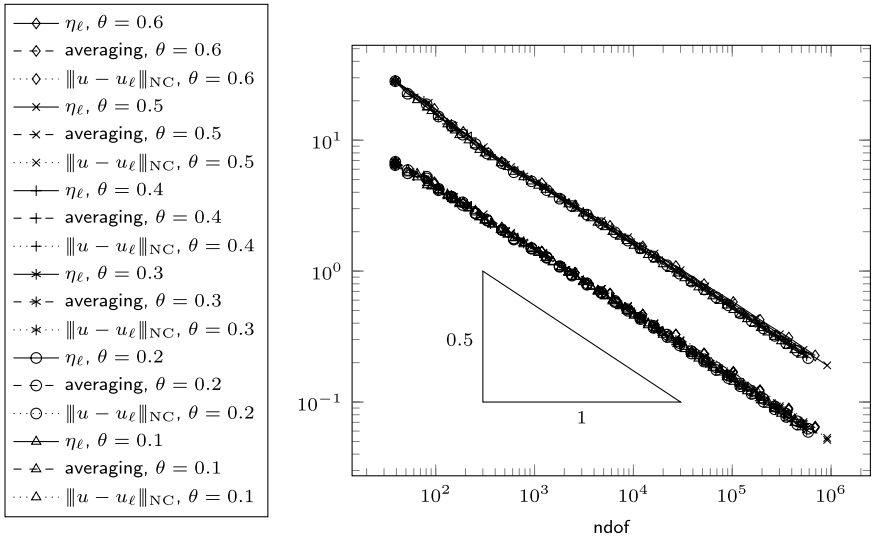

Fig. 9. Convergence history of the error and estimators for the 1/8 cusp domain with $\theta = 0.1, \ldots, 0.6$.

7.3. Domain with 1/8 cusp

On $\Omega := (-1, 1)^2 \backslash \mathrm{conv}\{(0, 0), (1, -1), (1, 0)\}$, the exact solution from [33, p. 107] is defined via (7.1) for the parameters $\alpha := 0.50500969$ and $\omega := 7\pi/4$. Figs. 8–9 show the convergence history of the error estimators and the exact error for uniform and adaptive meshes. The choice of $\theta \leq 0.5$ yields optimal convergence rates while larger values of θ or uniform refinement lead to sub-optimal convergence rates.

7.4. Domain with 1/16 cusp

On $\Omega := (-1, 1)^2 \backslash \mathrm{conv}\{(0, 0), (1, -0.5), (1, 0)\}$, the exact solution [33, p. 107] is given via (7.1) for the parameters $\alpha := 0.50060833$ and $\omega := 15\pi/8$. Figs. 10–11 show the convergence history of the error estimators and the exact error for uniform and adaptive meshes. As in the previous examples, the averaging error estimator yields a very accurate approximation of the true energy error.

Figs. 12–13 display the adaptive meshes for different values of θ. The adaptive mesh-refinement mainly concentrates on the re-entrant corner. In contrast to second-order problems, one can observe some additional refinement layers at the flat parts of the boundary.

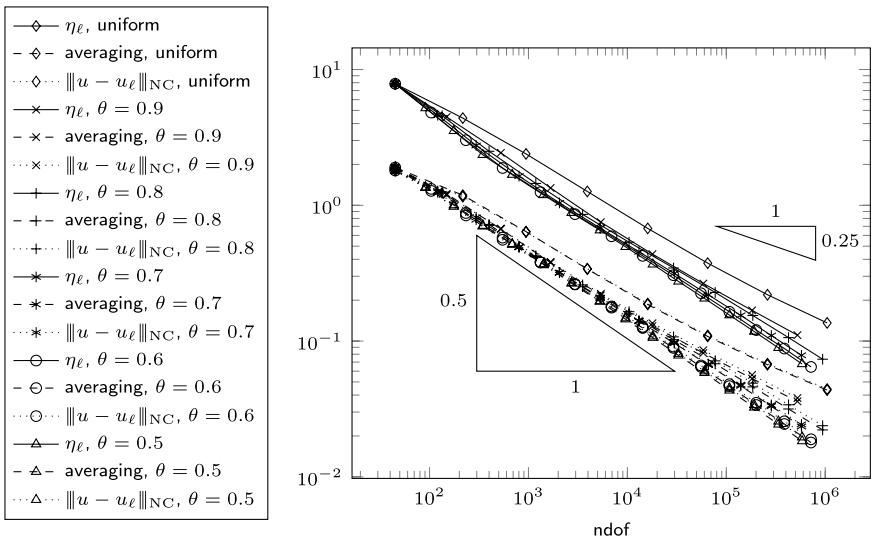

Fig. 10. Convergence history of the error and estimators for the 1/16 cusp domain with $\theta = 0.5, \ldots, 0.9$ and uniform mesh-refinement.

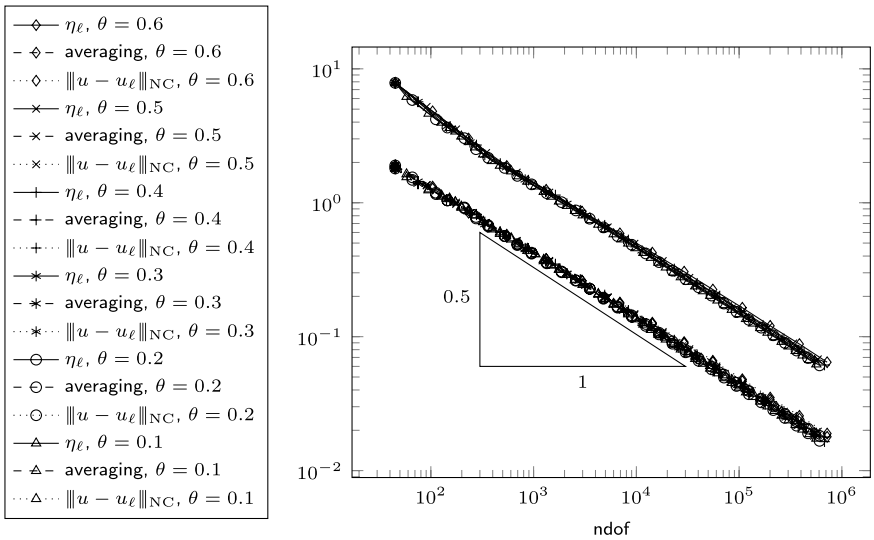

Fig. 11. Convergence history of the error and estimators for the 1/16 cusp domain with $\theta = 0.1, \ldots, 0.6$.

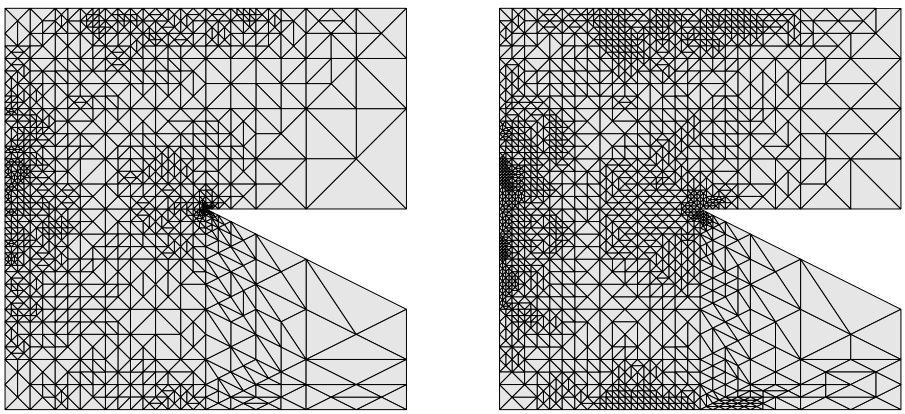

Fig. 12. Adaptive meshes for the 1/16 cusp example. Left: $\theta = 0.1$; level 23; 3582 degrees of freedom. Right: $\theta = 0.5$; level 8; 5267 degrees of freedom.

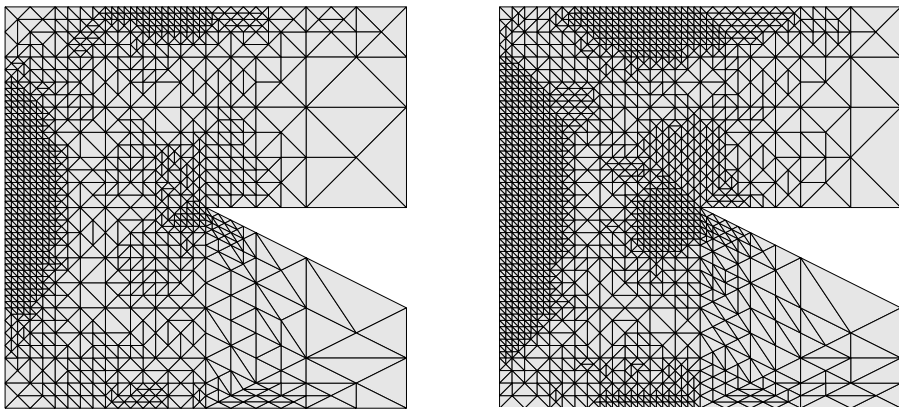

Fig. 13. Adaptive meshes for the 1/16 cusp example. Left: $\theta = 0.8$; level 5; 3628 degrees of freedom; Right: $\theta = 0.9$; level 5; 5393 degrees of freedom.

References

[1] X. Feng, R. Glowinski, M. Neilan, Recent developments in numerical methods for fully nonlinear second order partial differential equations, SIAM Rev. 55 (2) (2013) 205–267.
[2] X. Feng, M. Neilan, Analysis of Galerkin methods for the fully nonlinear Monge–Ampère equation, J. Sci. Comput. 47 (3) (2011) 303–327.
[3] M. Neilan, A nonconforming Morley finite element method for the fully nonlinear Monge–Ampère equation, Numer. Math. 115 (3) (2010) 371–394.
[4] D. Braess, Finite Elements. Theory, Fast Solvers, and Applications in Elasticity Theory, third ed., Cambridge University Press, Cambridge, 2007. Translated from the German by Larry L. Schumaker.
[5] P.G. Ciarlet, The Finite Element Method for Elliptic Problems, in: Studies in Mathematics and its Applications, vol. 4, North-Holland Publishing Co., Amsterdam, 1978.
[6] L.S.D. Morley, The triangular equilibrium element in the solution of plate bending problems, Aeronaut. Q. 19 (1968) 149–169.
[7] T. Gudi, A new error analysis for discontinuous finite element methods for linear elliptic problems, Math. Comp. 79 (272) (2010) 2169–2189.
[8] L. Beirão da Veiga, J. Niiranen, R. Stenberg, A posteriori error estimates for the Morley plate bending element, Numer. Math. 106 (2) (2007) 165–179.
[9] J. Hu, Z. Shi, A new a posteriori error estimate for the Morley element, Numer. Math. 112 (1) (2009) 25–40.
[10] L. Beirão da Veiga, J. Niiranen, R. Stenberg, A posteriori error analysis for the Morley plate element with general boundary conditions, Internat. J. Numer. Methods Engrg. 83 (1) (2010) 1–26.
[11] J. Hu, Z. Shi, J. Xu, Convergence and optimality of the adaptive Morley element method, Numer. Math. 121 (4) (2012) 731–752.
[12] R. Stevenson, Optimality of a standard adaptive finite element method, Found. Comput. Math. 7 (2) (2007) 245–269.
[13] J. Cascon, C. Kreuzer, R.H. Nochetto, K.G. Siebert, Quasi-optimal convergence rate for an adaptive finite element method, SIAM J. Numer. Anal. 46 (5) (2008) 2524–2550.
[14] C. Carstensen, M. Feischl, M. Page, D. Praetorius, Axioms of adaptivity, Comput. Math. Appl. 67 (6) (2014) 1195–1253.
[15] R. Becker, S. Mao, Z. Shi, A convergent nonconforming adaptive finite element method with quasi-optimal complexity, SIAM J. Numer. Anal. 47 (6) (2010) 4639–4659.
[16] R. Becker, S. Mao, Quasi-optimality of adaptive nonconforming finite element methods for the Stokes equations, SIAM J. Numer. Anal. 49 (3) (2011) 970–991.
[17] C. Carstensen, D. Peterseim, H. Rabus, Optimal adaptive nonconforming FEM for the Stokes problem, Numer. Math. 123 (2) (2013) 291–308.
[18] C. Carstensen, H. Rabus, The adaptive nonconforming FEM for the pure displacement problem in linear elasticity is optimal and robust, SIAM J. Numer. Anal. 50 (3) (2012) 1264–1283.
[19] J. Hu, J. Xu, Convergence and optimality of the adaptive nonconforming linear element method for the Stokes problem, J. Sci. Comput. 55 (1) (2013) 125–148.
[20] H. Rabus, A natural adaptive nonconforming FEM of quasi-optimal complexity, Comput. Methods Appl. Math. 10 (3) (2010) 315–325.
[21] J. Hu, Z. Shi, J. Xu, Convergence and optimality of the adaptive Morley element method, arXiv Preprint 1309.3606. http://arxiv.org/abs/1309.3606.
[22] C. Carstensen, D. Gallistl, M. Schedensack, Adaptive nonconforming Crouzeix–Raviart FEM for eigenvalue problems, Math. Comp. (2014), in press.
[23] J. Huang, X. Huang, Y. Xu, Convergence of an adaptive mixed finite element method for Kirchhoff plate bending problems, SIAM J. Numer. Anal. 49 (2) (2011) 574–607.
[24] P. Binev, W. Dahmen, R. DeVore, Adaptive finite element methods with convergence rates, Numer. Math. 97 (2) (2004) 219–268.
[25] R. Stevenson, The completion of locally refined simplicial partitions created by bisection, Math. Comp. 77 (261) (2008) 227–241.
[26] F. Brezzi, M. Fortin, Mixed and Hybrid Finite Element Methods, in: Springer Series in Computational Mathematics, vol. 15, Springer-Verlag, New York, 1991.
[27] L.R. Scott, S. Zhang, Finite element interpolation of nonsmooth functions satisfying boundary conditions, Math. Comp. 54 (190) (1990) 483–493.
[28] J. Alberty, C. Carstensen, S.A. Funken, Remarks around 50 lines of Matlab: short finite element implementation, Numer. Algorithms 20 (2–3) (1999) 117–137.
[29] M. Wang, J. Xu, The Morley element for fourth order elliptic equations in any dimensions, Numer. Math. 103 (1) (2006) 155–169.
[30] S.C. Brenner, C. Carstensen, Encyclopedia of Computational Mechanics, John Wiley and Sons, 2004 (Chapter 4, Finite element methods).
[31] S. Funken, D. Praetorius, P. Wissgott, Efficient implementation of adaptive P1-FEM in Matlab, Comput. Methods Appl. Math. 11 (4) (2011) 460–490.
[32] C. Carstensen, D. Gallistl, J. Hu, A posteriori error estimates for nonconforming finite element methods for fourth-order problems on rectangles, Numer. Math. 124 (2) (2013) 309–335.
[33] P. Grisvard, Singularities in Boundary Value Problems, in: Recherches en Mathématiques Appliquées (Research in Applied Mathematics), vol. 22, Masson, Paris, 1992.